International Journal of Gas Turbine, Propulsion and Power Systems
June 2024, Volume 15, Number 3

Numerical Investigation of Heat Transfer and Purge Flow Mechanisms in a Turbine Cascade with Bottom Platform Cavity

Marco Hahn[1], Jonas Schmid[1] and Hans-Jörg Bauer[1]

[1]Institute of Thermal Turbomachinery (ITS)
Karlsruhe Institute of Technology (KIT)
Kaiserstr. 12, 76131 Karlsruhe, Germany

ABSTRACT

The turbine of an aeroengine is exposed to a high-temperature mainstream, making sufficiently dimensioned cooling and sealing for all components involved indispensable. Balanced thermal safety and overall efficiency demand a better understanding of the aerodynamic and thermal behavior. This study focuses on the cavity at the bottom of the rotor platform, which is connected to the main flow through the midpassage gap between two adjacent blades mounted on the turbine disk. A numerical approach has been conducted to obtain the flow mechanism, sealing effectiveness and heat transfer characteristic for various purge flow rates and midpassage gap clearances. The results of the steady-state simulations show variations in the flow pattern and in the thermal load parameters, such as the adiabatic cooling effectiveness or the heat transfer coefficient. The distinct sensitivity highlights the necessity of a subtle adjustment of those parameters, to prevent critical hot spots endangering thermal safety.

NOMENCLATURE

a, b, d, h, t	Geometrical parameters, $[m]$
C	Chord length, $[m]$
L	Length, $[m]$
$\dot{m}$	Mass flow, $[kg/s]$
Ma	Mach number, $[-]$
Nu	Nusselt number, $[-]$
p	Pressure, $[Pa]$
Pr	Prandtl number, $[-]$
$\dot{q}$	Heat flux, $[W/m^2]$
Re	Reynolds number, $[-]$
s	Gap clearance, $[m]$
T	Temperature, $[K]$
Tu	Turbulence intensity, $[\%]$
u	Velocity in axial x-direction, $[m/s]$
v	Velocity in circumferential y-direction, $[m/s]$
w	Velocity in radial z-direction, $[m/s]$
x	Coordinate in axial direction, $[m]$
y	Coordinate in circumferential direction, $[m]$
z	Coordinate in radial direction, $[m]$
β	Flow angle, $[deg]$
η	Effectiveness, $[-]$
λ	Thermal conductivity, $[W/(m*K)]$

Manuscript Received on July 31, 2023
Review Completed on April 16, 2024

Abbreviations

CFD	Computational Fluid Dynamics
ITS	Institute of Thermal Turbomachinery
KIT	Karlsruhe Institute of Technology
PF	Purge Flow Rate
RANS	Reynolds-Averaged Navier Stokes

Subscripts

1	inlet
2	outlet
aw	adiabatic wall
ax	axial
c	cooling gas
cav	cavity
conv	convective
corr	corrected
f	fluid
hg	hot gas
max	maximum
mpg	midpassage gap
rim	rim seal
s	sealing
t	turbulent
w	wall
+	normalized

INTRODUCTION

To meet cost reduction goals and tightening climate targets, the primary optimization strategy of gas turbine applications aims to maximize efficiency. As a result, the turbine inlet temperature has increased to levels exceeding the melting temperature of the currently employed materials. The applied cooling and sealing technologies guarantee thermal safety during operation and are in the focus of recent research into aeroengine turbines. Air extracted from the high-pressure compressor is passed to the turbine and acts as cooling air and purge flow through cavities and gaps to concurrently prevent hot gas ingestion. Excess air ensures sufficient sealing and cooling but also reduces flow and thermodynamic efficiency while lacking air could result in hot gas ingestion and thus in a dangerous lifetime reduction. To elaborate an effective design of the cooling and sealing techniques, a broad understanding of secondary flow phenomena on the turbine platform, as captured by Wang et al. [1], is essential for aerodynamic performance and thermal safety. In recent years, many experiments and numerical studies were carried out on turbine passages, cavities and gaps to obtain profound understanding of flow and thermal characteristics [2].

A turbine geometry studied extensively is the rim seal between the turbine stator and rotor. Many studies focus on different geometric rim seal configurations at different purge flow rates. The

major aim is to assess the effect on the sealing effectiveness as well as aerodynamic losses and film cooling in the turbine passage [3,4]. In addition, some studies include the so-called midpassage gap between two adjacent platform segments. This gap shows a cooling potential for the platform and blades by fluid entering the turbine cascade. Therefore, these studies capture the interaction of the hot gas stream and the cooling purge flow and assess the influence on the cooling effectiveness [5–8]. Apart from these gaps, different cavities are located near the rim seal. Main issues in the analysis of such disk cavities are the heat transfer mechanism and again the sealing effectiveness to protect the disk from hot gas ingestion [9, 10].

All these studies neglect the influence of another cavity located at the bottom of the rotor platform between two adjacent blades, as indicated in Figure 1. The midpassage gap connects this bottom platform cavity with the turbine passage, enabling the interaction between the mainstream and purge flow. In Figure 2, the meridian section of a generic 1.5 turbine stage is shown. It illustrates a possible flow structure, where ingested hot gas of the mainstream mixes with the supplied purge flow, leading to strongly inhomogeneous mixing temperatures within the cavity. To the knowledge of the authors, there has not yet been any other study analyzing the mixing and flow in such a cavity underneath the turbine platform so far. However, an increased amount of hot gas ingestion through the midpassage gap causes an additional thermal load on the blade root where high centrifugal forces are already present. An excess of purge air, on the other hand, would increase thermodynamic and aerodynamic losses, leading to an optimization problem. For this reason, the following study focuses on the sealing effectiveness of the bottom platform cavity and thermal loads at the cavity walls to quantify the thermal safety risk by means of heat transfer parameters. To assess the sensitivity of these parameters, a parametric study of the purge flow rate and the midpassage gap clearance was performed and will be discussed in the following sections.

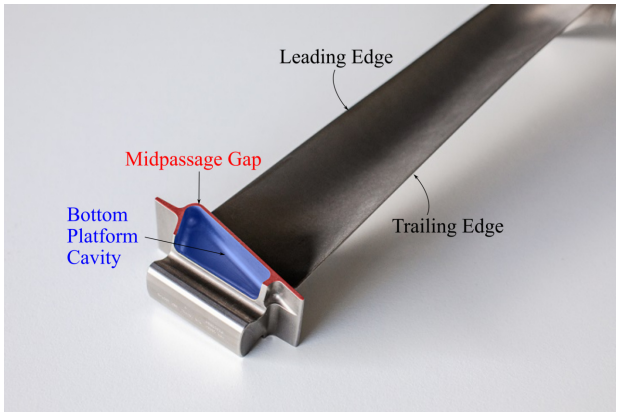

Fig.1: Bottom platform cavity and midpassage gap of two adjacent blades in a single GE9X turbine blade [11].

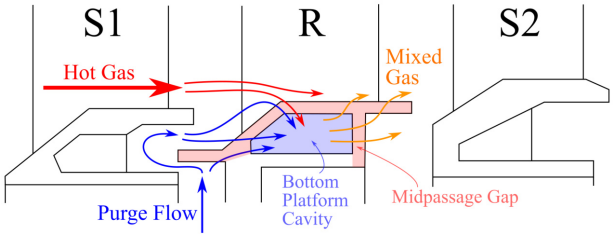

Fig.2: Meridian section of a generic 1.5 low-pressure turbine stage representing a possible flow configuration.

NUMERICAL METHODOLOGY

The numerical simulations were carried out with the commercial software *ANSYS CFX 2023 R1*, solving steady-state Reynolds-Averaged Navier Stokes (RANS) equations. The flow was considered compressible using the total energy heat transfer model including the viscous work term in the energy equation. To model turbulent viscosity, the k,omega-SST model was selected. Assuming an analogous turbulent transport for thermal and momentum diffusivity, the turbulent Prandtl number was set to $Pr_t = 0.9$. A high-resolution scheme was adopted for numerical discretization of the convective term. The medium was considered to be a perfect gas whose transport properties, such as dynamic viscosity and thermal conductivity, were calculated by Sutherland´s formula.

Computational domain and boundary conditions

The examined geometry is inspired by the rotor of a low-pressure turbine stage and has undergone geometrical simplifications. The dimensions of the bottom platform cavity are proportionate to the real engine's shape and remain constant throughout the entire investigation due to geometrical similarity reasons. In the future, numerical results will be validated with the pending experimental data of a new test rig with an implemented midpassage gap and rim seal at ITS. An examination of both experimental and computational results from a similar heat transfer configuration by Ranson et al. [12] demonstrated a substantial agreement. Moreover, Lynch and Thole [13] employed computational data to support the interpretation of the experimental findings. All geometric parameters are listed in Table 1 and mapped in Figures 3a and 3b. The test rig is designed as a linear turbine cascade. Therefore, linear periodicity is applied at the lateral boundaries for one pitch and rotational effects, such as a circumferential velocity component of the purge flow at the rim seal, are neglected. The cascade consists of purely prismatic blades, using the blade profile by Lorenz et al. [14] who analyzed the aerodynamic performance and thermal behavior of this blade in a linear turbine cascade [15].

An overview of the applied boundary conditions is given in Figure 4. The computational domain consists of two mass flow inlets and two averaged static pressure outlets for the hot gas and purge flow sections, respectively. The required blade span of the experimental test rig was captured in a preliminary CFD (Computational Fluid Dynamics) of the turbine cascade without any cooling supply ensuring no manipulation of the secondary flow system at the platform by the opposite flow system at the blade tip. To reduce the number of cells, only half of the derived blade span was simulated and a free-slip boundary condition was applied at mid-span. Another free-slip condition was adopted at the walls of the cooling outlet channel (see Figure 4) to prevent a pressure drop due to its extended length, ensuring a pressure level of the same magnitude for both outlets. Due to the angulated direction of the outlet channels, the blade wake can be traced for a distance of about $2.8C$, until the wake reaches the hot gas outlet boundary. At the remaining smooth walls of the passage, rim seal, midpassage gap and cavity, a no-slip boundary condition was applied.

In Table 2, the parameters of the boundary conditions are summed up. For each case (variations of the purge flow rate and midpassage gap clearance), the operation point is defined by mass flow-averaged Mach and Reynolds numbers at the exit of the turbine cascade close to the trailing edges of the airfoils, which were achieved by adjusting the inlet mass flow rates. Temperature and turbulence levels at the inlets were defined in due consideration of the similarity to a typical real engine. The analysis primarily centers around Plane 1, corresponding to the rim seal and midpassage gap, along with Surface 2, which corresponds to the opening gap of the bottom platform cavity (see Figure 3b).

Mesh characteristics and sensitivity

The mesh was generated with *Fidelity Pointwise 2022* using structured hexahedrons consistently to generate the best possible

mesh quality. The maximum skewness centroid was around 0.9 and the average skewness centroid of all hexahedrons below 0.1, representing a high orthogonality of the mesh. Some exemplary mesh regions are pictured in Figure 5, showing the rim seal, turbine passage and cavity. Next to walls with the no-slip boundary condition, the minimum cell height was chosen to have a y^+value below 1 during a first iteration procedure. To prevent an overestimation of the turbulent viscosity (and therefor an incorrect calculation of the turbulent diffusion) arising from an over-refined mesh, the $y^+ < 1$ condition is violated in adjacent gap regions, representing a negligible proportion of the total surface area. During a second iteration procedure, different growth ratios have been compared, resulting into a chosen growth ratio of 1.2. At relevant surfaces, a constant growth ratio for at least 15 cells is satisfied. To generate mesh-independent results, a prior mesh convergence study was conducted. For the operation point with a PF of 0.5%, the area-averaged adiabatic wall temperatures of the cavity and turbine cascade walls were compared for different numbers of total cells. During this last procedure, the height of the smallest cell as well as the growth ratio remained unchanged. The results indicate mesh-independent temperatures for the employed mesh with 46 million cells. This tested mesh was chosen for the parametric study of the purge flow to generate the later discussed results. For the parametric study of the midpassage gap clearance, a slightly different mesh with an equivalent number of cells has been generated to compare the influence of this geometrical variation.

Related parameters and data reduction

The sealing effectiveness and thermal load were analyzed by a parametric study of the purge flow rate PF (Table 2) defined as the ratio of the cooling flow $\dot{m}_c$ to the span-corrected mainstream flow $\dot{m}_{hg,corr}$:

$$PF = \frac{\dot{m}_c}{\dot{m}_{hg,corr}} \tag{1}$$

The sealing effectiveness is derived locally at the rim on control plane 1 (Figure 3b). It is defined by a normalized temperature including the hot gas temperature T_{hg} and the cooling temperature T_c and can also be interpreted as an inverse fluid temperature $T_+ = 1 - \eta_s$ [3]:

$$\eta_s = \frac{T_{hg} - T}{T_{hg} - T_c} \tag{2}$$

For evaluation of the thermal load, two different variables are derived, which are commonly used for film cooling analysis: The adiabatic cooling effectiveness η_{aw} and the Nusselt number Nu_f as dimensionless representation of the heat transfer coefficient are obtained by adding the chord length C and the thermal conductivity of the fluid λ_f to the equation:

$$\eta_{aw} = \frac{T_{hg} - T_{aw}}{T_{hg} - T_c} \tag{3}$$

$$Nu_f = \frac{\dot{q}_{conv}}{T_{aw} - T_w} \cdot \frac{C}{\lambda_f} \tag{4}$$

The application of these parameters is justified by the similarity to a film cooling configuration due to the hot gas ingestion through the midpassage gap into the bottom platform cavity and aligns to the superposition approach [16]. The reference temperature for this evaluation is defined by the adiabatic wall temperature T_{aw}, which is captured by a simulation with an adiabatic boundary condition at the walls. In contrast to this, the wall temperature T_w is captured by another non-adiabatic simulation with a heat flux boundary condition $\dot{q}_{conv}$ at the examined cavity walls. For this additional simulation the magnitude of the heat flux is set to $10 kW/m^2$ under consideration of a negligible variation in the flow field and transport properties for applicability of the superposition principle of film cooling.

Table 1: Geometric and aerodynamic parameters of the computational domain.

Geometrical Parameter	**Value**
True Chord Length	C
Axial Chord Length, C_{ax}	$0.89C$
Pitch, t	$0.75C$
Span, h	$0.48C$
Midpassage Gap Clearance, s_{mpg}	$0.005C - 0.01C$
Rim Seal Clearance, s_{rim}	$0.25C$
Cavity Dimensions, $a \cdot b \cdot d$	$L \cdot 0.56L \cdot 0.33L$
Relative Cavity Position, y_A/y_B	0.5
Inlet (Outlet) Flow Angle, β_1 (β_2)	63° (27.2°)
Hot Gas Inlet (Outlet) Length, $L_{hg,1}$ ($L_{hg,2}$)	$1.25C$ ($1.25C$)
Cooling Inlet (Outlet) Length, $L_{c,1}$ ($L_{c,2}$)	$0.5C$ ($5C$)

Table 2: Boundary conditions of the numerical computation.

Boundary Condition	**Value**
Mach Number, $\overline{Ma}$	0.5
Reynolds Number, $\overline{Re}$	$7.5 \cdot 10^5$
Temperature Ratio, T_{hg}/T_c	1.55
Purge Flow Rates, PF	$0.1\% - 2\%$
Turbulence Intensity, Tu	5%

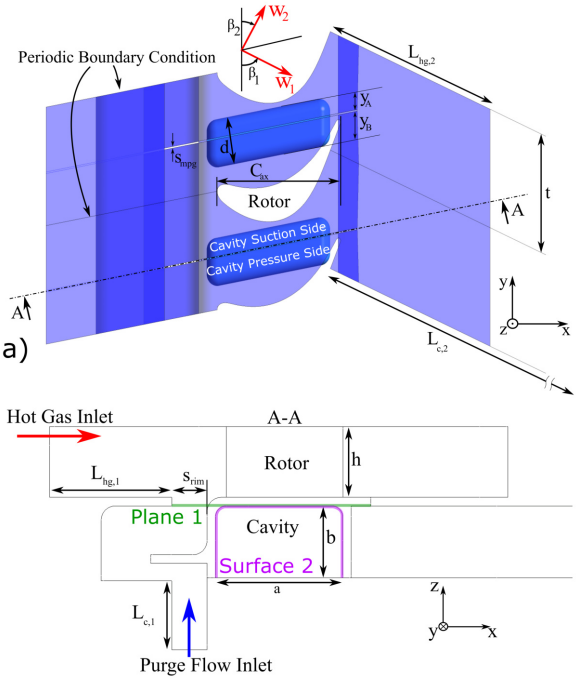

Fig.3: Schematic representation of the geometry of the computational domain: (a) Radial view; (b) section view along midpassage gap.

An identical approach was used by Zhang et al. [3] to derive a heat transfer coefficient.

RESULTS AND DISCUSSION

Concerning the flow field and normalized fluid temperature distribution presented in Figure 6, an initial evaluation of the perfusion behavior within the bottom platform cavity can be made. The plane under consideration is positioned along the midpassage gap

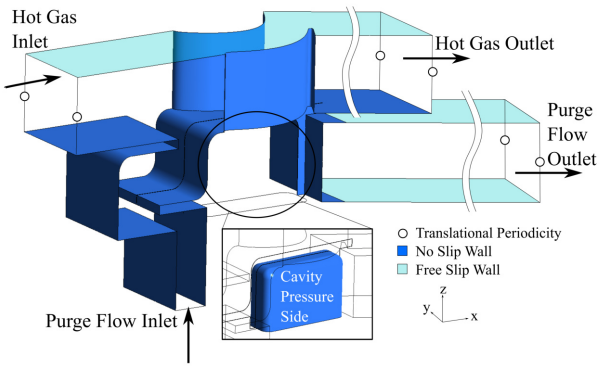

Fig.4: Schematic representation of the boundary conditions of the computational domain.

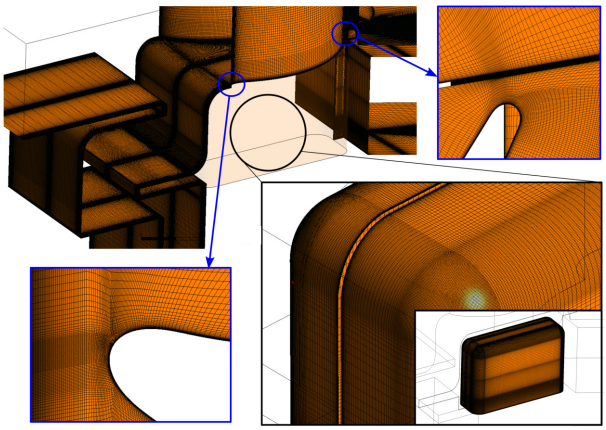

Fig.5: Visualization of the structured mesh of the computational domain with a focus on the leading edge, trailing edge and bottom platform cavity.

and aligns with the section depicted in Figure 3b. For the nominal operating conditions, a midpassage gap clearance of $s_{mpg} = 0.005C$ and a purge flow rate of $PF = 0.5\%$ were defined. While these parameters vary, the flow field and fluid temperature distribution undergo changes, yet the fundamental flow character of cavity perfusion remains consistent. The visual depiction of the flow field illustrates a complex perfusion pattern of the midpassage gap into the bottom platform cavity. Cold purge flow is introduced from the rim seal into the cavity at location A. At location B, the residual purge flow functions as sealing, protecting against the hot gas flow and forming a cooling film on the top side of the platform. However, an ingestion of mixing of hot gas and cooling flow occurs in the upstream region of the midpassage gap. Further downstream at location C, this ingestion turns into an egression of mixed fluids back into the turbine cascade. The temperature resulting from the mixing within the cavity shows a strongly inhomogeneous distribution and is the main factor determining the local heat transfer. In the subsequent sections, the impact of variations in the midpassage gap clearance and purge flow rate on hot gas ingestion and thermal load will be investigated.

Parameter sensitivity of hot gas ingestion

For the simulations in this study, the hot gas operation point is kept constant and the variation of the sealing behavior is analyzed for various purge flow rates PF and two different midpassage gap clearances s_{mpg}. For the PF variation, the main focus of this analysis is on the PF range from 0.25% to 0.75%. However, some quantitative depictions also include a PF variation from 0.1% to 2%. In Figure 7, the resulting velocities in radial z-direction (for each case divided by the absolute value of the highest velocity component in radial z-direction $|w|_{max}$ of plane 1) are visualized by means of contour plots for three different PF at plane 1 (see Figure 3b) and two different s_{mpg}. Areas marked in red in the contour plot represent ingestion of fluid into the interior, whereas areas in blue mark egression into the turbine cascade. The qualitative representation does not show significant variations in the velocity distribution along the midpassage gap. However, the area of egressing fluid into the cascade at position A between the stagnations points of two adjacent rotor blades increases slightly with rising PF. Since the pressure level in this area is lower than the area near the stagnation points, the fluid is more prone to egress rather than ingress. Comparing the two different gap clearances, the perfusion behavior shows an identical tendency. Just the case with the highest PF of the larger gap clearance still show ingestion of fluid, while fluid egression next to the midpassage gap is found for the smaller gap at position A. This almost negligible sensitivity is due to the fact that the purge rate is chosen as boundary condition, which is not a primarily independent value. The resulting mass flow rate and perfusion behavior are indeed determined by the applied pressure ratio and gap clearance. Consequently, the momentum ratio appears to be the actually determining and independent factor for the sensitivity of the hot gas ingestion. In the same visualization manner, Figure 8 shows the sealing effectiveness η_s at plane 1. In contrast to the previous depiction, the sealing effectiveness level exhibits a global increase with rising PF. In addition, the location of the maximum of the sealing effectiveness within the rim seal seems to vary slightly due to a change of PF and s_{mpg}, which was not the case for the velocity component in radial z-direction. Comparing the two different gap clearances with identical PF, the smaller s_{mpg} shows higher values of η_s at the rim seal and midpassage gap area, reflecting a better protection against hot gas ingestion. Hence, the intuitive assumption that a smaller gap with a high PF implies the best protection against hot gas ingestion is confirmed. A more quantitative consideration of the perfusion behavior is visualized in Figure 9a. For different PF and s_{mpg} combinations, this figure shows the normalized velocity component in radial z-direction along the midsection of the midpassage gap. To compare the perfusion behaviors of the midpassage gap of all cases, the velocity component in radial z-direction of the respective case was normalized by dividing it by the respective absolute value of the highest velocity component along the midsection. For each case, this value was located at approximately 0.8 of the relative gap length. The perfusion behavior shows two slight shifts with varying PF and s_{mpg} along the midpassage gap: Firstly, a first change of direction at position A is shifted upstream with

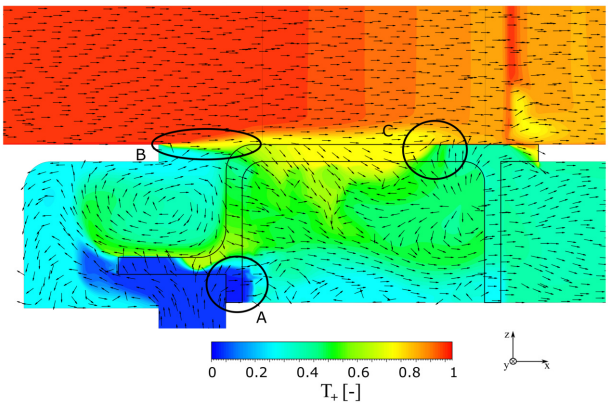

Fig.6: Flow field and temperature distribution of the nominal operation point in a section view along the midpassage gap.

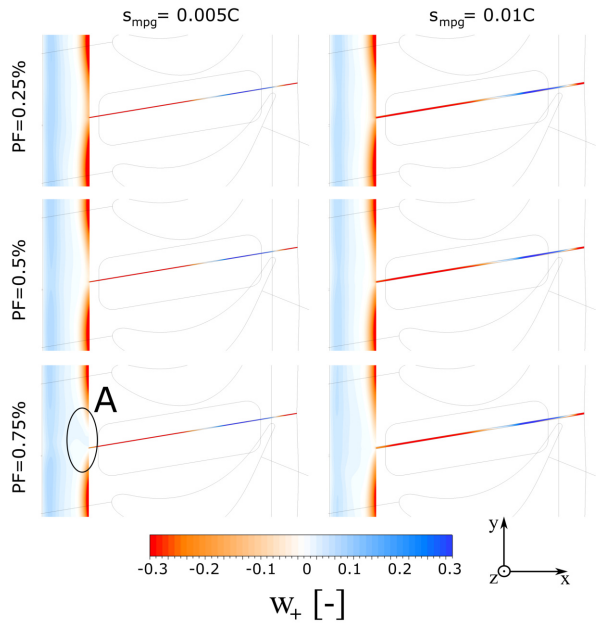

Fig.7: Normalized velocity in radial direction $w_+ = w/|w|_{\max}$ distribution for various PF and two different s_{mpg} at plane 1.

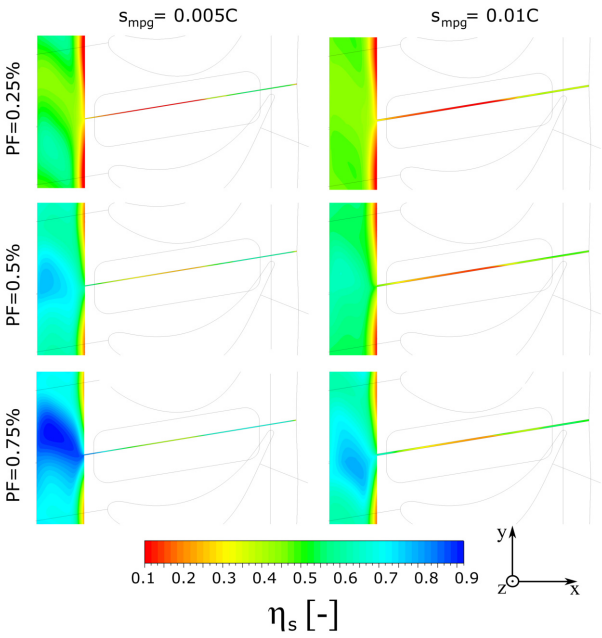

Fig.8: Sealing effectiveness η_{s} distribution for various PF and two different s_{mpg} at plane 1.

increasing PF and decreasing s_{mpg}. The comparison of the area-averaged pressures in the cavity $\overline{p}_{\mathrm{cav}}$ for different PF shows that a higher PF leads to an increased $\overline{p}_{\mathrm{cav}}$. Considering the acceleration along the turbine passage, which leads to a continuous pressure drop, this upstream shift of a change in direction can be explained by the pressure in the cavity exceeding the pressure in the passage earlier. In addition, a larger gap clearance also leads to an increased $\overline{p}_{\mathrm{cav}}$ in the bottom platform cavity. This behavior can be explained by a larger amount of cooling air, entering a larger midpassage gap. It acts like a rising PF and also increases the pressure level in the bottom platform cavity. However, the perfusion of the gap behaves differently, since the first shift in direction moves downstream with bigger gap clearances, although $\overline{p}_{\mathrm{cav}}$ is rising. Thus, an exclusive consideration of the pressure level in the cavity does not explain this behavior. Some possible explanatory approaches could be a change in the secondary flow system within the turbine cascade or an alteration of the flow structure through the larger midpassage gap due to the higher amount of cooling air in the bottom platform cavity. Regarding a standardized pressure distribution of the hot gas facing platform, some minor differences are found, which confirm this interpretation. Another explanation could also be the connection to the purge flow outlet channel, which could also interact differently due to a change in the gap width. In the region downstream of the cavity location at position B, a second change of direction can be detected, which seems to be independent of PF (position B). Therefore, this second change is likely not affected by the bottom platform cavity and can be explained by the influence of the pressure level of the purge flow outlet channel. For all simulations, this pressure level is adjusted to the pressure level of the turbine cascade (the same averaged static pressure at both outlets), leading to a pressure below the pressure in the bottom platform cavity. Thus, an earlier protection against hot gas ingestion into the bottom platform cavity has changed to a second location of ingestion into the purge flow outlet channel. In contrast to the PF, a variation in s_{mpg} indeed affects the area downstream of the cavity location. With smaller gap clearance, the shift of direction moves upstream. This behavior could also be a result of a change in the secondary flow system or of the wake of the turbine blade passing the midpassage gap, which interacts differently with the purge flows of different gap clearances. This explanation is based on the fact that the standardized pressure distribution at the wake position also differs for different cases. Considering the variations of the absolute values of the radial velocity component w, a change of PF results in negligible variations, whereas a change to the bigger gap clearance increases the maximum value at plane 1 by approximately 25%. Regarding the amount of fluid moving through the complete length of the midpassage gap in all cases, the locations where fluid gets ingested into the cavity show higher mass flow values than the regions where fluid gets egressed. This is due to elevated velocities at the locations of hot gas ingestion (also considering the u and v components of the velocity). Since a variation in PF does not change the perfusion behavior downstream of the bottom platform cavity, it can be concluded that a variation in PF mainly changes the pressure level in the bottom platform cavity, which in turn influences the perfusion of the gap region connected to the cavity. However, a modification of the gap clearance influences the flow situation such that it cannot be solely explained by considering the pressure in the bottom platform cavity. The flow rather depends on the pressure field distribution at the hot gas-facing platform wall, which determines the whole perfusion behavior. For a final assessment of the total sealing effectiveness, the area-averaged sealing effectiveness at plane 1 and surface 2 (see Figure 3b) for both s_{mpg} and various PF is plotted in Figure 9b. As expected, the sealing behavior increases steadily with rising PF and also shows higher values for smaller s_{mpg}, leading to a greater protection against hot gas ingestion. Comparing the two different control surfaces, the area-averaged total sealing effectiveness is consistently higher at plane 1 than on surface 2 due to the big area at the rim seal upstream of the midpassage gap, where cold fluid gets egressed. Considering the perfusion of the cavity (surface 2), a bigger gap clearance results in a slightly higher deviation between plane 1 and surface 2 than the smaller gap clearance. As a consequence, an already lower sealing behavior at plane 1 due to a bigger gap clearance leads to an even worse sealing behavior in therms of the cavity perfusion, with this sensitivity being higher for bigger gap clearances. For the overall sensitivity of hot gas ingestion, it can be concluded that a variation of PF or s_{mpg} causes some differences in the locations of the changes in direction of the fluid and also in the amplitude of the absolute velocity component in radial direction. Therefore, the perfusion behavior can be varied

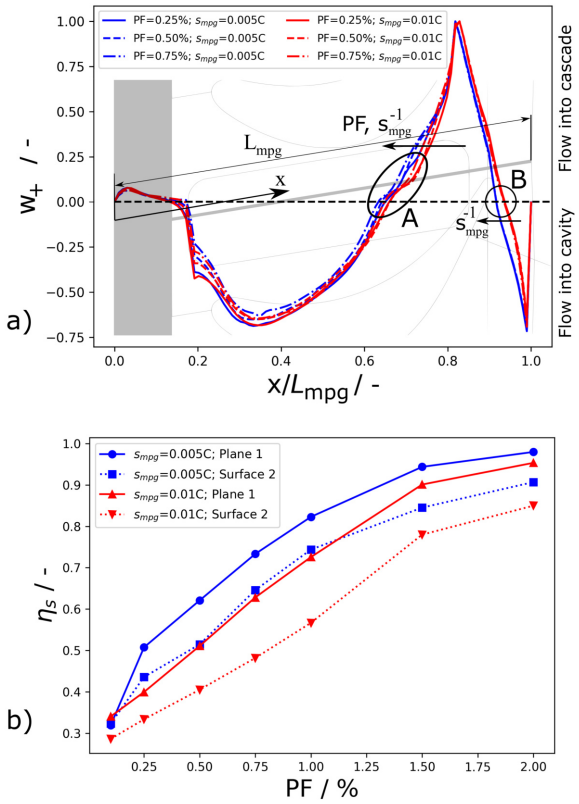

Fig.9: Assessment of hot gas ingestion: (a) Normalized velocity in radial direction $w_+ = w/|w|_{\max}$ for various PF and s_{mpg} along the midpassage gap direction; (b) Area-averaged sealing effectiveness for various PF and s_{mpg} at plane 1 and surface 2.

by the parameters of this sensitivity study. In addition, the sealing effectiveness and, hence, thermal protection of the interior exhibit remarkable variations, which should be taken into account during the design process.

Parameter sensitivity of thermal load

Considering the same simulations as for the ingestion study, the variation in the sealing behavior can also be analyzed by its effect on adiabatic cooling effectiveness within the turbine cascade. In Figure 10 the adiabatic cooling effectiveness on the platform side facing the hot gas in the turbine cascade is plotted for different PF and s_{mpg}. With an increase of the PF, adiabatic cooling effectiveness rises steadily and also the totally cooled area is further distributed compared to small PF. However, the shape of the cooled area is similar for all PF and shows the tendency of the platform facing the hot gas being cooled better next to the suction side of the airfoil,whereas cooling of the area next to the pressure side of the airfoil is worse. This is due to the fact that the egressed purge flow is sucked to the suction side as a result of the pressure gradient towards the suction side. Considering the variation of s_{mpg}, the global level of cooling is higher with a smaller gap clearance. Having a more detailed look into the contour plots, some subtle distinctions at the downstream end of the midpassage gap are visible: On the one hand, the small gap clearance causes a higher adiabatic cooling effectiveness for the lowest PF than the large clearance with the highest PF at location A on the wall facing the hot gas. On the other hand, location B represents a small hot spot for all smaller clearances, which is not that pronounced in cases with a larger gap clearance. This might be explained by the earlier observed second change in the perfusion

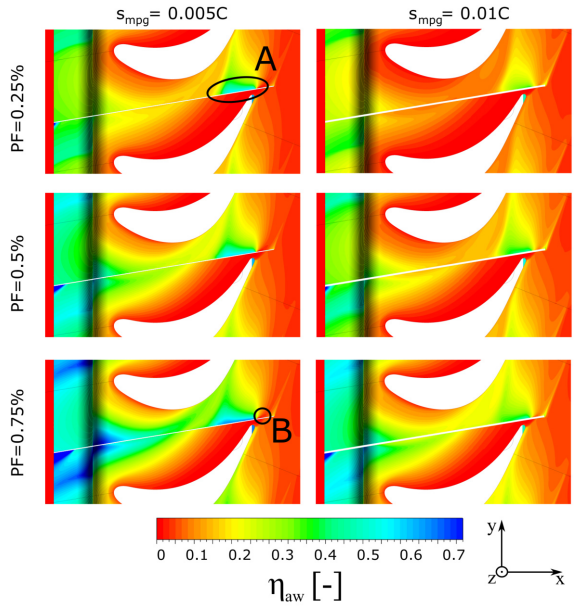

Fig.10: Cooling effectiveness distribution η_{aw} for various PF and two different s_{mpg} at the platform wall facing the hot gas.

direction (location C in Figure 9a). For the larger gap clearance, the location of this change of direction was located further downstream, which now leads to a wider spread of the cooled area and a less pronounced hot spot at location B. On a global scale, the bigger gap clearance produces a less distributed cooling area, but does not show a specific hot spot. An analog visualization of adiabatic cooling effectiveness on the cavity suction side and top walls is presented in Figure 11. For a clearer representation of the thermal parameter variation, the scaling of the contour plot differs from that of the previous depiction of Figure 10. At the cavity walls on the pressure side, thermal parameters show significantly lower values and a much more homogeneous distribution. Similarly to the passage flow, the ingested purge flow appears to be pulled to the cavity wall on the suction side. The pressure field within the turbine cascade seems to globally affect fluid flow in the cavity. With respect to the larger variations of thermal parameters, this study focuses on the suction side of the cavity and the top walls. As expected, adiabatic cooling effectiveness in the lower half exceeds that in the upper half of the cavity. This is due to the fact that fresh purge air is blown into the lower part of the cavity, whereas already mixed gas is sucked into the upper part of the cavity. Two regions can be distinguished in the contour plots: Firstly, a well-cooled area at the bottom of the cavity (corresponding to location B) and secondly, a badly cooled region at the top wall (corresponding to location A). By increasing the PF, the well-cooled region becomes even more defined, whereas the badly cooled area is gradually smoothed. Compared to the small gap clearance, the large gap produces another behavior at an increasing purge flow rate: At location A, adiabatic cooling effectiveness decreases with rising PF from 0.25% to 0.5% and at position B, adiabatic cooling effectiveness also decreases with a further increase in PF from 0.5% to 0.75%.This variation in the cooling pattern for different gap clearances shows the complexity and sensitivity of the perfusion behavior in the bottom platform cavity.

To investigate heat transfer, the ingestion and cooling studies in the PF range from 0.25% to 0.75% were extended by simulations with an additional heat flux boundary condition at the cavity walls. Using Equation 4, the Nusselt number was derived for the cavity´s suction side and top walls, as indicated in Figure 12. For various PF, all distributions show the highest heat transfer values in the upstream part of the cavity at location A. Another heat transfer hot spot

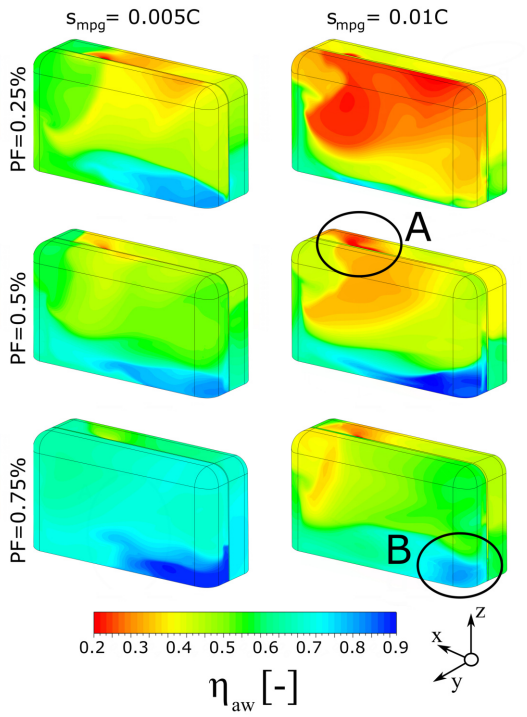

Fig.11: Cooling effectiveness distribution η_{aw} for various PF and two different s_{mpg} on the cavity´s suction side and top walls.

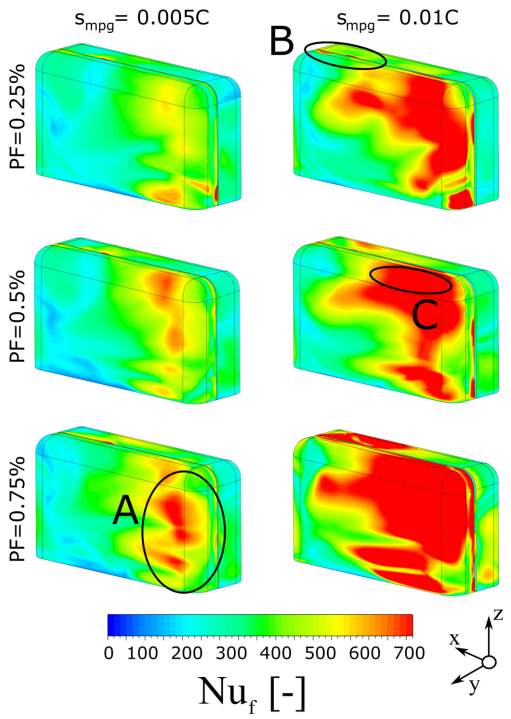

Fig.12: Derived Nusselt numbers Nu_f for different PF and s_{mpg} on the cavity suction side and top walls.

is located at position B. This location corresponds to the first shift of direction, where perfusion changes from hot gas ingested into the cavity to mixed air egressing into the turbine cascade. Investigation of the heat transfer mechanisms reveals a steady increase of the Nusselt number as well as a further distributed area with higher values of PF and s_{mpg}. The magnitude of the Nusselt number for the bigger gap clearance must be noted. It is significantly higher than the magnitude of the lower gap clearance. For a comprehensive analysis of the thermal load, Nusselt number distribution has to be analyzed in combination with the adiabatic cooling effectiveness plots. Since higher PF also correspond to a higher Nusselt number, it can be concluded that the heat transfer mechanism in the cavity is primarily driven by the purge flow ingested into the cavity. However, there are locations in the bottom platform cavity, which concurrently show a high Nusselt number and a low adiabatic cooling effectiveness. These regions are the critical areas in the bottom platform cavity and are mostly located in the top part of the cavity´s suction side wall close to the midpassage gap (locations B and C in Figure 12). At these positions, hot gas ingestion takes place, leading to a higher thermal load on the cavity walls by less mixed hot gas at the high temperature of the turbine cascade. The control of those locations will be crucial in the dimensioning process of the bottom platform cavity. For assessment of the overall thermal load, the area-averaged total adiabatic cooling effectiveness for all cavity walls and passage walls as well as the total Nusselt number for all cavity walls are plotted in Figure 13. Both thermal parameters show a continuous increase with rising PF. A comparison of the cavity walls with the cascade walls (see Figure 13a) shows a higher adiabatic cooling effectiveness of the latter due to included areas in the cascade, where no cooling air reaches the surface. The bigger clearance consistently produces lower adiabatic cooling effectiveness values over the whole range of the different PF. Especially in the PF range from 0.25% to 1.25%, the difference of this thermal parameter is noticeable. For very low and very high PF values, the difference in adiabatic cooling effectiveness for the two gap clearances can be neglected. In contrast to this, the area-averaged total Nusselt number in Figure 13b consistently shows higher values for the bigger gap clearance. Remarkably, the steadily increasing gradient also seems to be higher for the bigger gap clearance, which leads to the conclusion that this s_{mpg} is more sensitive to a variation in PF. At a PF value of 0.75%, the Nusselt number rises to values that are far higher than for the other cases.

CONCLUSION

This numerical study covered the flow mechanisms and heat transfer characteristics in a turbine cascade with a bottom platform cavity. From varying the purge flow rates and the midpassage gap clearance, the following main conclusions can be derived with respect to the aerodynamic and thermal behavior:

1. With increasing PF, the sealing effectiveness rises continuously. For the highest PF of 2% investigated, a decreasing gradient in the sealing effectiveness is found, indicating saturation.

2. A smaller gap clearance results in a better protection against hot gas ingestion.

3. Comparing the behaviors of perfusion through the midpassage gap, two shifts can be detected: A first change of direction is shifted upstream with rising PF and decreasing s_{mpg}. As a result, hot gas ingestion is reduced and the cooled area on the top platform wall expands. Additionally, a second shift of direction downstream of the cavity area can be detected, which seems to be independent of the PF. Depending on the location of this second shift in direction (influenced by s_{mpg}), small hot spots may develop in the adiabatic cooling effectiveness plots of the platform wall facing the hot gas.

4. The thermal parameters and their variations on cavity´s suction side and top walls exceed those in the cavity´s pressure side wall.

5. The maximum values of the Nusselt number are found in the upstream area of the cavity suction side wall and in the top

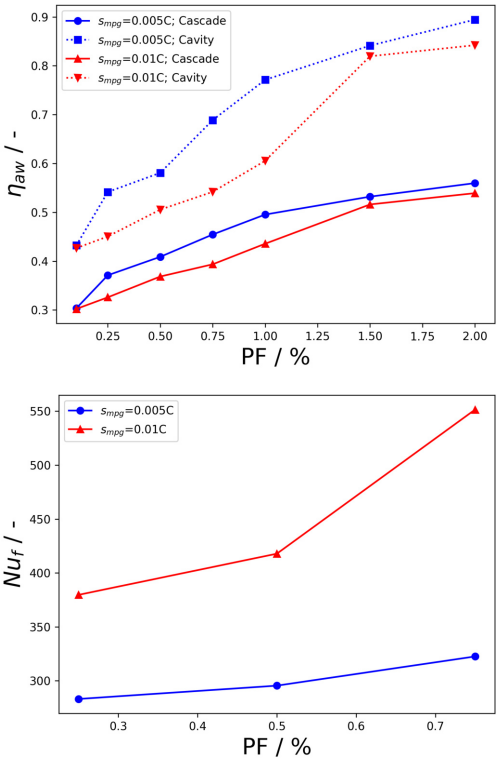

Fig.13: Assessment of the thermal load for various PF: (a) area-averaged adiabatic cooling effectiveness η_{aw} at the cavity walls and the remaining walls in the passage; (b) area-averaged Nusselt number Nu_f at all cavity walls.

wall region at the location of the first shift in direction through the midpassage gap. The most critical locations in therms of thermal load are in the top wall region next to the midpassage gap, where high Nusselt numbers correlate with low adiabatic cooling effectiveness values.

6. The total adiabatic cooling effectiveness and Nusselt number are globally increasing with rising PF. Additionally, a higher gap clearance is more sensitive to a variation of PF than smaller gap clearances.

This study presents the initial exploration of the bottom platform cavity connected to the turbine cascade via the midpassage gap. To validate the numerical findings, it is imperative to compare them with experimental data. The aerodynamic and thermal data required for this validation process will be obtained from a newly established test rig at ITS.

ACKNOWLEDGEMENTS

The investigations presented in this publication were carried out within the research program LuFo VI-1 HoATT. The work was supported by the Federal Ministry for Economic Affairs and Climate Action (BMWK) as per resolution of the German Federal Parliament under grant number 20T1907. The authors gratefully acknowledge MTU Aero Engines for support and permission to publish this paper.

REFERENCES

[1] Wang, H. P., Olson, S. J., Goldstein R. J. and Eckert E. R. G., 1997, "Flow Visualization in a Linear Turbine Cascade of High Performance Turbine Blades", *ASME Journal of Turbomachinery*, Vol. 119(1): 1-8 (8 pages).

[2] Barigozzi, G., Abdeh, H., Rouina, S. and Franchina, N., 2022, "The Aero-Thermal Performance of Purge Flow and Discrete Holes Film Cooling of Rotor Blade Platform in Modern High Pressure Gas Turbines: A Review", *MDPI Int. J. Turbomach. Propuls. Power*, Vol. 7(3), 22.

[3] Zhang, Z., Zhang, Y., Zhang, Y., Dong, X. and Lu, X., 2022, "Numerical investigation of the purge flow mechanisms and heat-transfer characteristics of turbine rim seals", *Elsevier Ltd. Case Studies in Thermal Engineering*, Vol 40, 102484.

[4] Mansouri, Z., 2021, "Aerodynamic and heat transfer performances of highly loaded transonic turbine rotor with upstream generic rim seal cavity", *KeAi Propulsion and Power Research*, Vol 10(4), pp. 317-331.

[5] Park, S., Sohn, H.-S., Shin, S., Ueda, O., Moon, H. K. and Cho, H. H., 2021, "Film cooling characteristics on blade platform with a leakage flow through mid-passage gap", *Elsevier Ltd. International Journal of Heat and Mass Transfer*, Vol 167, 120800.

[6] Lynch, S. P. and Thole, K. A., 2017, "Heat Transfer and Film Cooling on a Contoured Blade Endwall With Platform Gap Leakage", *ASME Journal of Turbomachinery*, Vol. 139(5): 051002 (10 pages).

[7] Hada, S. and Thole, K. A., 2011, "Computational Study of a Midpassage Gap and Upstream Slot on Vane Endwall Film-Cooling", *ASME Journal of Turbomachinery*, Vol. 133(1): 011024 (9 pages).

[8] Shaikh, F. and Rosic, B., 2022, "Aerodynamics and Heat Transfer Inside a Gas Turbine Mid-Passage Gap", *ASME Journal of Turbomachinery*, Vol. 144(4): 041010 (9 pages).

[9] Paniagua, G., Dénos, R. and Almeida, S., 2004, "Effect of the Hub Endwall Cavity Flow on the Flow-Field of a Transonic High-Pressure Turbine", *ASME Journal of Turbomachinery*, Vol. 126(4): 578-586 (9 pages).

[10] Patinios, M., Scobie, J. A., Sangan, C. M. and Lock, G. D., 2017, "Performance of Rim-Seals in Upstream and Downstream Cavities over a Range of Flow Coefficients", *MDPI Int. J. Turbomach. Propuls. Power*, Vol. 2(4), 21.

[11] Davies, S., "GE Aviation GE9X engine receives FAA certification", TCT Magazine, https://www.tctmagazine.com/additive-manufacturing-3d-printing-news/ge-aviation-ge9x-engine-receives-faa-certification/.

[12] Ranson, W. W., Thole, K. A. and Cunha, F. J., 2005, "Adiabatic Effectiveness Measurements and Predictions of Leakage Flows Along a Blade Endwall", *ASME Journal of Turbomachinery*, Vol. 127(3): 609-618 (10 pages).

[13] Lynch, S. P. and Thole, K. A., 2011, "The Effect of the Combustor-Turbine Slot and Midpassage Gap on Vane Endwall Heat Tranfer", *ASME Journal of Turbomachinery*, Vol. 133(4): 041002 (9 pages)

[14] Lorenz, M., Schulz, A. and Bauer, H.-J., 2012, "Experimental Study of Surface Roughness Effects on a Turbine Airfoil in a Linear Cascade – Part II: Aerodynamic Losses", *ASME Journal of Turbomachinery*, Vol. 134(4): 041007 (10 pages).

[15] Lorenz, M., Schulz, A. and Bauer, H.-J., 2012, "Experimental Study of Surface Roughness Effects on a Turbine Airfoil in a Linear Cascade – Part I: External Heat Transfer", *ASME Journal of Turbomachinery*, Vol. 134(4): 041006 (11 pages).

[16] Choe, H., Kays, W. M. and Moffat, R. J., 1974, "The Superposition Approach to Film-Cooling", *ASME Winter Annual Meeting*, New York, N.Y., Nov. 17-22, 10 p.